05

Formation of plasma periodic structures in the volume of fused silica exposed by focused laser radiation with a wavelength of 1030 nm

© A.V. Bogatskaya [1,2], A.M. Popov [1,2]

[1] Moscow State University,
119991 Moscow, Russia
[2] Lebedev Physical Institute, Russian Academy of Sciences,
119991 Moscow, Russia

e-mail: annabogatskaya@gmail.com

Received December 11, 2023
Revised January 09, 2024
Accepted January 16, 2024

Femtosecond laser writing of birefringent subwavelength nanostructures in dielectrics has been studied for almost two decades since it is of interest for a number of practical applications such as optical memory, optical waveguides, microfluidic channels, etc. In this work, a numerical modeling of the formation of plasma periodic nanostructures in fused silica in the direction of propagation of a focused laser beam is carried out. It is shown that the focused beam creates a plasma layer with a supercritical concentration of electrons which provides an effective reflection of the incident laser pulse, leading to the formation of a standing wave of ionization. Effective ionization occurs in the bungles of wave, that forms a plasma lattice with a period equal to the period of the standing wave in the medium. Modeling allows us to determine the conditions under which the proposed regime of nanostructuring is possible.

Keywords: laser microstructuring in dielectrics, birefringent nanostructures, fused silica, electron-hole plasma, nano- and micromodifications, multiphoton ionization in strong fields.

DOI: 10.61011/EOS.2024.01.58289.15-24

Introduction

Huge efforts have been made in recent decades to study the key features of the microscale surface and volumetric modifications of materials induced by focused femtosecond laser pulses [1–3]. Steady progress of powerful ultrafast laser facilities identifies new interaction mechanisms between field, plasma and material subsystems resulting in various types of structural modifications in transparent dielectrics such as micropores and nanopores and material compaction zones [4–7], periodic changes in refraction index [8–10], modification due to phase transitions [11], etc. Specific interest to fused silica has emerged after study [12] where possible recording of birefringent volumetric nanostructures was demonstrated for the first time. Later studies in volumetric nanostructure physics conducted by a number of research teams [13,14] have identified several main mechanisms such as incident radiation interference with the formed plasma wave [4,12], formation of plasma nanoscale structures due to the local field amplification followed by self-ordering in nanoplane along the laser propagation direction [15,16], superfast exciton-polariton self-trapping [17].

A recent study [18] proposed an alternative mechanism of volume nanograting formation. The mechanism involves interference of incident and reflected light waves in a focal area of the beam (within spatial laser pulse length) with generation of plane standing wave and corresponding plane wave of material ionization (plasma „sheet“ stacks). Further excitation and interference of surface plasmons propagating towards each other at the boundary of ionized and non-ionized dielectric layers causes periodic subwavelength variations of the refraction index along the laser pulse polarization resulting in formation of birefringent nanostructures within a solid dielectric [19,20].

The predicted modality was in the best way implemented in lithium niobate [21], however, this mechanism appears to be equally applicable to a wide range of dielectrics because it involves only generation and further evolution of electron-hole plasma. Experimental findings of Kudryashov's team [21] have shown that these subwavelength nanomodifications along the laser beam axis are observed in pre-filamentation mode of laser pulse focusing.

The absence of strict theoretical models supporting the proposed mechanism and of clear understanding of the mechanism implementation conditions prevents further progress of laser recording of such birefringent nanostructures. Thus, the objective of the study is to provide numerical simulation of laser-induced solid-state plasma behavior within the predicted model to identify the key features of formation and scaling of extended birefringent structures depending on the focusing radiation.

Simulation of focused laser radiation propagation together with electron-hole plasma behavior

The plasma sheet generation mode predicted in [18] involves quite narrow intensity range as a result of radiation reflection from the focal plasma. Thus, formation of

reflecting (postcritical) plasma in the beam focal plane requires high powers, however, according to the experimental data, and the absence of laser filamentation shall be provided simultaneously. In addition, the given mode will be quite sensitive to laser beam focusing parameters: on the one hand, strong focusing provides a high quality plane plasma mirror, on the other hand, to form more extended modification area, the longitudinal dimension of effective laser radiation shall be increased and this may be achieved at long focal waist lengths. For 1030 nm radiation, the threshold filamentation power may be assessed as follows

$$P_{\text{cr}} = \frac{3.72\lambda_0^2}{8\pi n_0 n_2}.$$

Here, λ_0 is the laser radiation wavelength, n_0 and n_2 are linear and nonlinear portions of refraction index calculated as follows $n = n_0 + n_2 I$ (I is the laser radiation intensity). By assuming $n_2 \approx 2.5 \cdot 10^{-16}\,\text{cm}^2/\text{W}$ [22], we get $P_{\text{cr}} = 4.3\,\text{MW}$ for 1030 nm. For a pulse width of 0.3 ps, this is approximately equal to $1.4\,\mu\text{J}$.

This study, simulates the propagation of focused subpicosecond laser pulse in fused silica together with generation and evolution of electron-hole plasma as well as further pulse reflection from the focal plasma with formation of a series of plasma sheets.

Some studies analyzed this problem in parabolic approximation (approximation of slowly changing amplitudes [23]) (see, for example, [24,25], where diffraction divergence and possible beam filamentation are also addressed). We cannot use such approach herein because significant reflection from the focal plasma layer will play a leading role in formation of a complex field structure induced by the interference of incident and reflected laser fields. To verify the proposed experimental mode of plasma sheet formation and to determine the laser exposure range that will help develop a more complicated 3D numerical model in future, herein we use a (quasi)one-dimensional approach similar to that used to study the microwave breakdown in atmosphere [26]. Similar to [26], the simulation addresses beam focusing by multiplying the wave field by a so called geometrical factor to identify the effective ionization region. It is important to stress that the one-dimensional simulation is applicable to this problem in the focal waist area ($z < z_f$) because the beam cross-section there varies weakly and the wave front may be assumed as approximately plane (this fact is described in detail in [27]).

The laser radiation parameters used in simulation are primarily defined by the capabilities of the current experiment. In particular, the possible focal waist range corresponds to fundamental harmonic laser pulse focusing of Satsuma femtosecond ytterbium optical fiber laser with $\lambda_0 = 1030\,\text{nm}$ by microlenses with various numerical apertures $NA = 0.45$, 0.55, 0.25 used by Lebedev Physical Institute RAS for laser microstructuring experiments [18–21]. The intensity range is also defined by the energies and pulse widths available for the experiments in pre-filamentation mode (pulses with energy up to $1.3\,\mu\text{J}$ and width $\tau_p = 0.3\,\text{ps}$ (FWHM)). Recent analysis in [28] has shown that the intensity range necessary for efficient sample ionization is within $10-100\,\text{TW/cm}^2$. Since the pulse repetition rate for the experiment is quite low ($\sim 100\,\text{kHz}$) compared with diffusion and recombination times in plasma, behavior of the excited electrons in dielectric may be addressed independently for each individual laser pulse. For the purpose of simulation, we divide the plasma stage of nanograting formation along laser beam propagation into two parts. In the first part, formation of high-reflective plasma mirror in the focal plane is addressed. Then, we analyze formation of plasma gratings as a result of interference of the incident and reflected laser waves from the focal plasma. At this stage, we solve (quasi)one-dimensional second-order wave equation, including, in particular, radiation absorption in the formed plasma layers.

In quasi-one-dimensional approximation, the first part of the problem may be written as to equations for charge carrier density N_e in the conduction and intensity band of laser radiation propagating in fused silica (laser beam focusing will be considered by introducing a geometrical factor that will be addressed below):

$$\frac{\partial N_e}{\partial t} = D\frac{\partial^2 N_e}{\partial z^2} + (N_{at} - N_e)\left[W_i(I) + \frac{N_e}{N_{at}}\nu_i\right] - \frac{N_e}{t_r}, \quad (1)$$

$$\frac{dI(z,t)}{dt} - \frac{c}{n_0}\frac{dI(z,t)}{dz} = \frac{cI_i}{n_0}(N_{at} - N_e)\left[W_i(I) + \frac{N_e}{N_{at}}\nu_i\right]. \quad (2)$$

Here, $I(z,t)$ is the radiation intensity (laser beam is assumed to move right to left), D is the electron diffusion constant that was assessed as $D \sim \frac{V_f^2}{3\nu_{tr}} \approx 300\,\text{cm}^2/\text{s}$, where $V_f \approx 10^8\,\text{cm/s}$ is the Fermi velocity, ν_{tr} is the transport collision frequency. Typical electron recombination time in fused silica is $t_r = 150\,\text{fs}$ [29], $\frac{c}{n_0}$ is the speed of light in fused quartz ($n_0 \approx 1.45$ is the refraction index), $N_{at} = 2.1 \cdot 10^{22}\,\text{cm}^{-3}$ is the atom density, $I_i = 9\,\text{eV}$ is the band gap. Ionization probability $W_i(I)$ in fused silica is calculated within the Keldysh model [30]. As is known, depending on the Keldysh parameter γ, the ionization process may be considered in terms of tunnel or multiphoton mode. Since the given intensity range is within $\gamma \sim 1$, our calculations use this general Keldysh expression as specified in [28]. Here, we also consider the laser ionization with frequency

$$\nu_i = \frac{1}{I_i}\frac{4\pi e^2 I(z,t)\nu_{tr}}{m^* c n_0(\omega_0^2 + \omega_{tr}^2)},$$

where $m^* = 0.5m_e$ is the effective carrier mass in the fused silica. It should be noted that for the fused silica, the effective mass is within $(0.5-1)m_e$ [31]. For the purpose of calculations, we use $0.5m_e$ without loss of generality. As has been mentioned above, beam focusing is considered by introducing the geometrical factor $F(z - z_0)$ in the

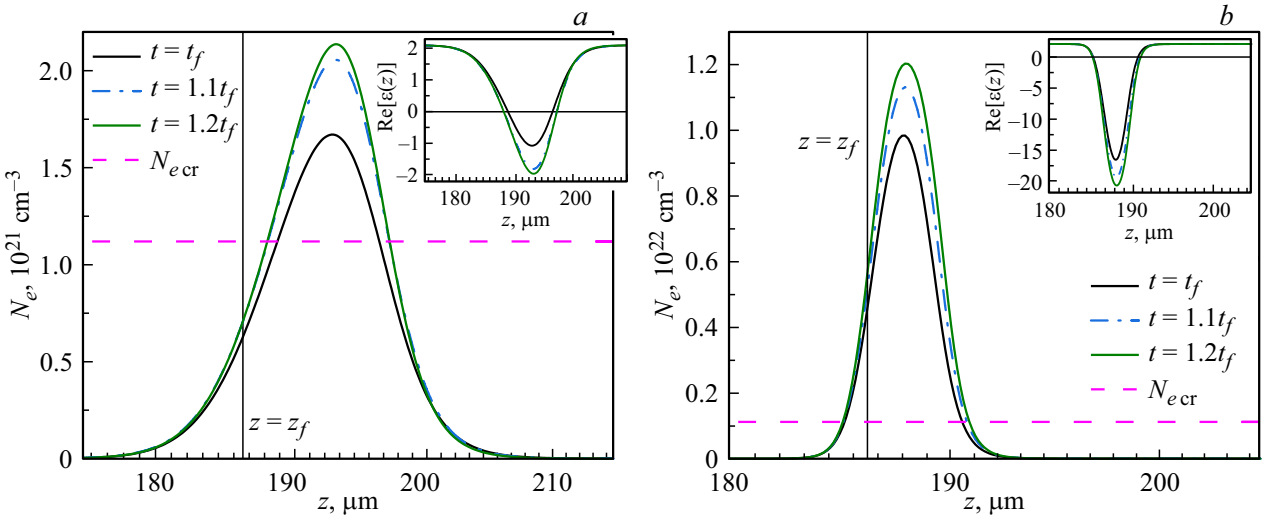

Figure 1. Temporal evolution of the electron density of the reflecting layer formed in the focal plane by 1030 nm laser radiation at various beam focusing parameters (strong focusing cases): $NA = 0.45$ (a), $NA = 0.55$ (b). Horizontal dashed curves denote critical plasma density ($N_{e\,\mathrm{cr}} = 1.12 \cdot 10^{21}$ cm^{-3} for 1030 nm). The Details show evolution of the real part of the plasma permittivity (7) in the appropriate points of time. Laser pulse parameters for the corresponding numerical apertures are shown in the Table.

expression for intensity:

$$I(z,t) = I_0 \exp\left(-\frac{(z - z_0 + \frac{c}{n_0}t)^2}{a^2}\right) F^2(z - z_f), \qquad (3)$$

$$F(z - z_f) = \sqrt{1\Big/\left(1 + \left(\frac{z - z_f}{l_f}\right)^2\right)}. \qquad (4)$$

Here, I_0 is the peak intensity of beam in the focusing area defined through the pulse energy W_p as

$$I_0 = \frac{W_p}{\tau S_0 \sqrt{\pi}}, \qquad (5)$$

where $\tau = \tau_p/2 = an_0/c$ is FWHM, $S_0 = \pi r_0^2$ is the focusing spot size. In (3), z_0 describes the initial beam position, z_f is the focal plane position, l_f is the Rayleigh length that is defined by the focal spot radius $l_f = \frac{\pi n_0 r_0^2}{\lambda_0}$ (hereinafter we chose focal radii corresponding to various numerical apertures $NA = 0.55, 0.45, 0.25$ [32–34], Table).

To analyze the second part of the problem, i.e. pulse reflection from the focal plasma layer, we integrate the Helmholtz equation together with the kinetic equation for electrons (1) in the specified standing wave field $E(z)$:

$$\frac{\partial^2 E(z)}{\partial z^2} + \frac{\omega_0^2}{c^2}\varepsilon(z)E(z) = 0. \qquad (6)$$

here, the initial dielectric permittivity profile $\varepsilon(z)$ is defined by electron distribution $N_e(z)$ in the reflecting layer (Figure 1):

$$\varepsilon(z) = n_0^2 - \frac{4\pi e^2 N_e(z)}{m(\omega_0^2 + \nu_{tr}^2)} + i\,\frac{\nu_{tr}}{\omega_0}\,\frac{4\pi e^2 N_e(z)}{m(\omega_0^2 + \nu_{tr}^2)}, \qquad (7)$$

where $\omega_0 = 2\pi c/\lambda_0$ is the radiation frequency.

Solution of equation (6), including the permittivity (7), provides a standing wave profile in whose antinodes effective ionization of the fused silica takes place. Wave field that defines the ionization process in equation (1) is derived from field $E(z)$ by multiplying by the geometrical factor (4). The following solution of equation (1) with the specified reflected wave field distribution defines the new dielectric permittivity profile (7). Then the Helmholtz equation (6) solution procedure is repeated. The described algorithm is used to simulate the formation and further evolution o plasma nanograting profiles in the laser pulse propagation direction. The algorithm was implemented using Wolfram Mathematica software suite. Whole lifetime of the reflected wave was assessed as $\tau_p/2$ — the interference time of the incident and reflected components of the pulse (here we assume that the effective reflection occurs at the time of focusing of the central beam portion — t_f as shown in the Table). It is important to noted that beam reflection simulation with plane-wave approximation appears to be feasible because the spatial pulse size in the given conditions is much higher than the length of the focal beam waist that defines the effective laser exposure area. Actually, for a pulse width of 0.3 ps, the spatial size is defined as $2a \approx 60\,\mu\mathrm{m} \gg l_f$ (Table).

Discussion

Figure 1 shows the data for formation of the reflecting plasma layer for 1030 nm radiation in various laser beam propagation times for two numerical apertures corresponding to strong focusing: $NA = 0.45$ (a) and 0.55 (b). The Details in the Figure show real parts of the dielectric permittivity of plasma in corresponding points of time. It is shown that the post-critical plasma is formed approximately

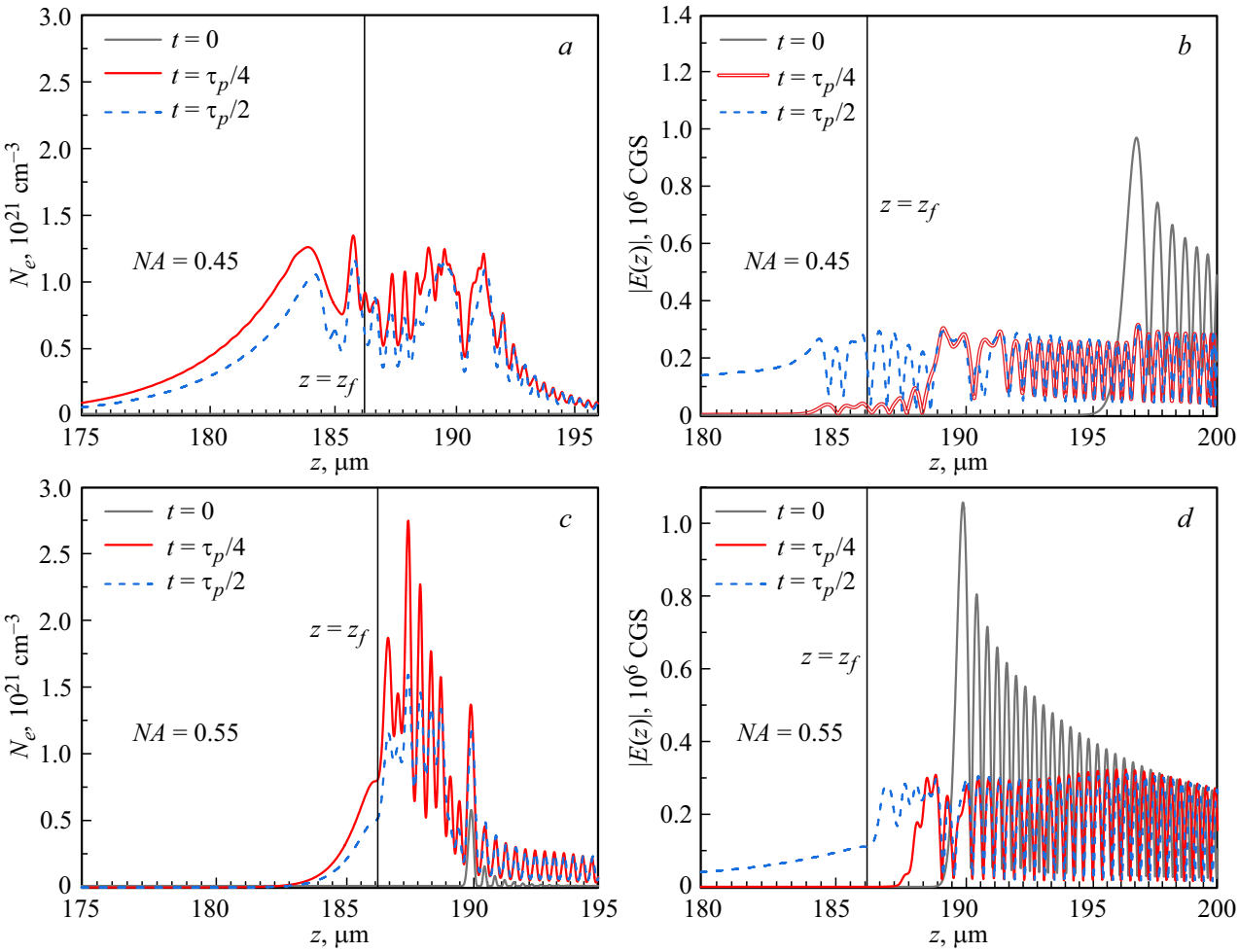

Figure 2. Plasma grating profiles formed along the 1030 nm laser pulse propagation as a result of wave rereflection from the focal layer (*a,c*), and corresponding standing wave field distributions (*b,d*) in different times after formation of the „primary" plasma layer for numerical apertures $NA = 0.45$ (*a,b*) and $NA = 0.55$ (*c,d*). Focusing radiation parameters are taken from the Table.

at t_f that corresponds to focusing of the central beam part. It is important that at stronger focusing, the formed plasma layer is much narrower and the electron concentration in it is almost an order of magnitude higher. Thus, to form a high quality plasma mirror, a stronger focusing is more preferable.

Figure 2 shows further results of plasma grating simulation with reflection from the formed plasma mirror based on the simultaneous solution of equations (6) and (7) with the corresponding distributions of reflected wave field. It is shown that in case of stronger focusing ($NA = 0.55$), the electron concentration level in the formed plasma layers is higher, however, the spatial length of the structure is much lower. Data analysis in Figure 2 shows that the subwavelength period of the formed gratings is more than the standing wave period $\lambda_0/2n_0$. Actually, in case of highly ionized material, the real part of the refraction index will differ considerably from n_0. For example, for electron concentration $\sim 10^{21}$ cm^{-3} and $\lambda_0 = 1030$ nm, the real part of the refraction index in the fused silica

Radiation focusing parameters

$\lambda_0 = 1030$ nm		
$\tau_p = 0.3$ ps $a \approx 30\,\mu$m $z_0 = 8a$ $z_f = 6a$ $t_f = \frac{(z_0 - z_f)}{c/n_0} = 3 \cdot 10^{-13}$ s		
$NA = 0.45$ $W_p = 1\,\mu$J $r_0 = 1.6\,\mu$m $l_f = 11.3\,\mu$m	$NA = 0.55$ $W_p = 0.45\,\mu$J $r_0 = 0.8\,\mu$m $l_f = 2.8\,\mu$m	$NA = 0.25$ $W_p = 2.5\,\mu$J $r_0 = 3.18\,\mu$m $l_f = 44.7\,\mu$m

may be estimated as $n' = 0.45$. This is consistent with the experimental data [20] where the measured period of longitudinal nanostructures appears to be close to $\lambda_0/2n'$, where $n' = \mathrm{Re}\left[\sqrt{\varepsilon(z)}\right]$.

We believe that sudden changes in the carrier concentration during laser exposure resulting in the change in

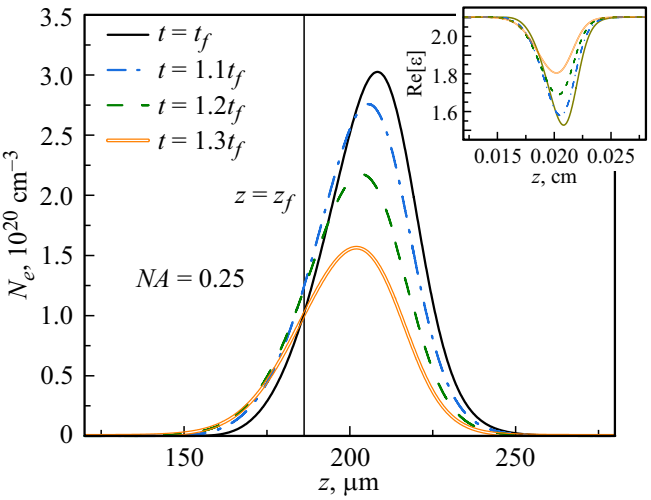

Figure 3. Temporal evolution of the electron density of the plasma layer formed in the focal plane by the 1030 nm laser pulse during focusing by a microlens with the numerical aperture $NA = 0.25$. The Detail shows the evolution of the real part of the plasma permittivity for these times. The pulse parameters are shown in the Table.

nanograting period may hinder the observation of periodicity in the real experiment. It should be also stressed that the described model does not consider diffraction effects in reflection that may result in angular beam scattering and loss of radiation coherence that, in turn, may result in smearing of standing wave antinodes and, therefore, reduce the „contrast" of nanograting periodicity.

To analyze the best parameters of radiation focusing, we provide below the reflecting plasma layer formation data for a longer radiation focusing case. Such focusing corresponds to the numerical aperture $NA = 0.25$ (Table). Here, the pulse energy is assumed equal to $W_p = 2.5\,\mu$J to ensure the pulse radiation intensity in the appropriate frequency range ($I_0 \sim 3 \cdot 10^{13}$ W/cm^2) for a higher beam radius (see equation (5)). Comparison of the reflecting layer behavior in Figure 1 and 3 suggests that the focal plasma layer becomes wider at longer focusing, however, the electron concentration in it does not achieve the critical value that prevents formation of contrast periodic structures in the laser propagation direction.

Thus, it is suggested that the plasma sheet formation mode is associated with strict focusing conditions. On the other hand, the length of effective interaction between laser radiation and dielectric substance reduces with decrease in the focal waist, that will result in reduction of structure length along the z axis (Figure 2). This will hinder the experimental observation and characterization of such structures. Thus, the best focal waist lengths that are necessary to achieve contrast plasma gratings shall be $\sim 10\,\mu$m.

In summary, it should be noted that fast progress in physics of superfast laser-induced self-organized nanostructuring in transparent dielectrics give the green light to various quantum technology applications and to creation of new types of metamaterials and optical memory elements. Formation of periodic volumetric nanostructures is also of special interest [35–37] because it facilitates the development of new theories and physical models for interpreting experimental data and effective control of structural modification periods.

However, particular contribution of various processes such as optical scattering, interference and field amplification during interaction between field and plasma subsystems in laser microstructuring is still poorly studied. The authors believe that the results of this study will help separate a special investigation area associated with the proposed interference mechanism of modification in subfilament mode that, together with the current experimental studies, will be useful for creation of reproducible periodic nanostructures with capability of handling the period, size and homogeneity of self-organizing modifications.

Conclusion

Numerical analysis of the effect of focused laser radiation in the volume of fused silica has been performed to verify the proposed mechanism of plasma sheet formation during laser pulse reflection from plasma occurring in the focal region. Simulation has been used to define the conditions under which the given nanostructuring mode can be achieved. In particular, it has been shown that strong focusing of laser beam is required to form contrast plasma gratings.

This study makes an important step towards understanding of the complex problem of modification mechanisms in solid bodies and of the processes behind them. This will, in future, bring us closer to the development of an advanced theoretical model for efficient control of microscale laser recording in solid dielectrics.

Funding

This study was financially supported by the Russian Science Foundation (project № 22-72-10076).

Conflict of interest

The authors declare that they have no conflict of interest.

References

[1] E. Mazur, R. Gattass. Nature Photon., **2**, 219–225 (2008). DOI: 10.1038/nphoton.2008.47
[2] R.S. Taylor, C. Hnatovsky, E. Simova, R. Pattathil. Opt. Lett., **32** (19), 2888-2890 (2007). DOI: 10.1364/OL.32.002888
[3] N.M. Bulgakova, V.P. Zhukov, S.V. Sonina, Y.P. Meshcheryakov. J. Appl. Phys., **118** (23), 233108 (2015). DOI: 10.1063/1.4937896
[4] Y. Shimotsuma, K. Hirao, J.R. Qiu, P.G. Kazansky. Mod. Phys. Lett. B, **19**, 225 (2005). DOI: 10.1142/S0217984905008281

[5] H.Y. Sun, J. Song, C.B. Li, J. Xu, X.S. Wang, Y. Cheng, Z.Z. Xu, J.R. Qiu, T. Jia. Appl. Phys. A, **88**, 285 (2007). DOI: 10.1007/s00339-007-4012-y
[6] M. Beresna, M. Gecevičius, N.M. Bulgakova, P.G. Kazansky. Opt. Express, **19**, 18989 (2011). DOI: 10.1364/OE.19.018989
[7] Y. Dai, A. Patel, J. Song, M. Beresna, P.G. Kazansky. Opt. Express, **24**, 19344 (2016). DOI: 10.1364/OE.24.019344
[8] C.B. Schaffer, A. Brodeur, J.F. García, E. Mazur. Opt. Lett., **26**, 93 (2001). DOI: 10.1364/OL.26.000093
[9] Z. Wang, K. Sugioka, Y. Hanada, K. Midorikawa. Appl. Phys. A, **88**, 699 (2007). DOI: 10.1007/s00339-007-4030-9
[10] A. Mermillod-Blondin, I.M. Burakov, Y.P. Meshcheryakov, N.M. Bulgakova, E. Audouard, A. Rosenfeld, A. Husakou, I.V. Hertel, R. Stoian. Phys. Rev. B, **77**, 104205 (2008). DOI: 10.1103/PhysRevB.77.104205
[11] V. Koubassov, J. Laprise, F. Théberge et al. Appl. Phys. A, **79**, 499–505 (2004). DOI: 10.1007/s00339-003-2474-0
[12] Y. Shimotsuma, P.G. Kazansky, J.R. Qiu, K. Hirao. Phys. Rev. Lett., **91**, 247405 (2003). DOI: 10.1103/PhysRevLett.91.247405
[13] R. Desmarchelier, B. Poumellec, F. Brisset, S. Mazerat, M. Lancry. World J. Nano Sci. Eng., **5**, 115–125 (2015). DOI: 10.4236/wjnse.2015.54014
[14] N.M. Bulgakova, V.P. Zhukov, Yu.P. Meshcheryakov. Appl. Phys. B, **113** (3), 437-449 (2013). DOI: 10.1007/s00340-013-5488-0
[15] V.R. Bhardwaj, E. Simova, P.P. Rajeev, C. Hnatovsky, R.S. Taylor, D.M. Rayner, P.B. Corkum. Phys. Rev. Lett., **96**, 057404 (2006). DOI: 10.1103/PhysRevLett.96.057404
[16] R. Taylor, C. Hnatovsky, E. Simova. Laser Photonics Rev., **2**, 26 (2008). DOI: 10.1002/lpor.200710031
[17] M. Beresna, M. Gecevičius, P.G. Kazansky, T. Taylor, A. Kavokin. Appl. Phys. Lett., **101**, 053120 (2012). DOI: 10.1063/1.4742899
[18] S.I. Kudryashov, P.A. Danilov, M.P. Smaev, A.E. Rupasov, A.A. Ionin, R.A. Zakoldaev. JETP Lett., **113**, 493–497 (2021). DOI: 10.1134/S0021364021080075
[19] S.I. Kudryashov, P.A. Danilov, A.E. Rupasov, M.P. Smayev, A.N. Kirichenko, N.A. Smirnov, A.A. Ionin, A.S. Zolot'ko, R.A. Zakoldaev. Appl. Surf. Sci., **568**, 150877 (2021). DOI: 10.1016/j.apsusc.2021.150877
[20] S. Kudryashov, A. Rupasov, R. Zakoldaev, M. Smaev, A. Kuchmizhak, A. Zolot'ko, M. Kosobokov, A. Akhmatkhanov, V. Shur. Nanomaterials, **12**, 3613 (2022). DOI: 10.3390/nano12203613
[21] S. Kudryashov, A. Rupasov, M. Kosobokov, A. Akhmatkhanov, G. Krasin, P. Danilov, B. Lisjikh, A. Abramov, E. Greshnyakov, E. Kuzmin et al. Nanomaterials, **12**, 4303 (2022). DOI: 10.3390/nano12234303
[22] D. Milam. Appl. Optics, **37** (3), 546-550 (1998). DOI: 10.1364/AO.37.000546
[23] S.A. Akhmanov. Sov. Phys. Usp., **29**, 589 (1986). DOI: 10.1070/PU1986v029n07ABEH003456
[24] A. Couairon, L. Sudrie, M. Franco, B. Prade, A. Mysyrowicz. Phys. Rev. B, **71**, 125435 (2005). DOI: 10.1103/PhysRevB.71.125435
[25] J. Hoyo, A. de la Cruz, E. Grace, A. Ferrer, J. Siegel, A. Pasquazi, G. Assanto. J. Solid. Sci. Rep., **5**, 7650 (2015). DOI: 10.1038/srep07650
[26] V.E. Semenov, E.I. Rakova, M.Yu. Glyavin, G.S. Nusinovich. Phys. Plasmas, **23** (7), 073109 (2016). DOI: 10.1063/1.4958313
[27] V.B. Gildenburg, I.A. Pavlichenko. Nanomaterials, **10** (8), 1461 (2020). DOI: 10.3390/nano10081461
[28] A. Bogatskaya, Yu. Gulina, N. Smirnov, I. Gritsenko, S. Kudryashov, A. Popov. Photonics, **10**, 515 (2023). DOI: 10.3390/photonics10050515
[29] P. Audebert, Ph. Daguzan, A. Dos Santos, J.C. Gauthier, J.P. Geindre, S. Guizard, G. Hamoniaux, K. Krastev, P. Martin, G. Petite, A. Antonetti. Phys. Rev. Lett., **73** (14), 1990 (1994). DOI: 10.1103/PhysRevLett.73.1990
[30] L.V. Keldysh. JETP, **20**, 1307–1314 (1964).
[31] N.M. Bulgakova, V.P. Zhukov, S.V. Soninam, Yu.P. Meshcheryakov. J. Appl. Phys., **118**, 233108 (2015). DOI: 10.1063/1.4937896
[32] Yu.S. Gulina, S.I. Kudryashov, N.A. Smirnov, E.V. Kuzmin. Opt. Spectrosc., **130** (4), 390 (2022). DOI: 10.21883/EOS.2022.04.53724.45-21
[33] G.K. Krasin, M.S. Kovalev, P.A. Danilov, N.G. Stsepuro, E.A. Oleynichuk, S.A. Bibicheva, V.P. Martovitskii, S.I. Kudryashov. JETP Lett., **114**, 117–123 (2021). DOI: 10.1134/S0021364021150054
[34] G.K. Krasin, M.S. Kovalev, S.A. Kudryashov, P.A. Danilov, V.P. Martovitskii, I.V. Gritsenko, I.M. Podlesnykh, R.A. Khmelnitskii, E.V. Kuzmin, Yu.S. Gulina, A.O. Levchenko. Appl. Surf. Sci., **595**, 153549 (2022). DOI: 10.1016/j.apsusc.2022.153549
[35] Y. Lu, Y. Li, X. Xie, Z. Tang, L. Li, J. Li, Y. Ding. Front. Chem., **10** (2022). DOI: 10.3389/fchem.2022.1082651
[36] B. Zhang, X. Liu, J. Qiu. J. Materiomics, **5** (1), 1–14 (2019). DOI: 10.1016/j.jmat.2019.01.002
[37] B. Zhang, Z. Wang, D. Tan et al. PhotoniX, **4**, 24 (2023). DOI: 10.1186/s43074-023-00101-8

Translated by E.Ilinskaya